

Polarization Insensitive and Thin Metamaterial Absorber Performed in High-Frequency 5G Bands

Seher Şeyma ARSLAN MADAK¹, Ahmet TEBER^{2*}, Ramazan TOPKAYA¹

Highlights:

- High frequency of 5G band metamaterial absorber is designed
- An absorption is achieved more than 87.6% from 24.20-27.30GHz
- The suggested absorber is low-cost and facile, which is useful in 5G high frequency applications

Keywords:

- mmWave absorber
- 5G
- Polarization insensitive
- Facile design

ABSTRACT:

A variety of fascinating applications, including 5G communication devices, high-speed data transfer, and large-scale Internet of Things (IoT), make life easier with 5G technology. Despite the 5G's superior features, the percentage of electromagnetic (EM) waves in the environment execute a significant increase, unpleasantly. Broadband metamaterial absorbers are an appealing alternative to gather these unwanted signals. This study aims to numerically investigate a broadband metamaterial absorber (MMA) in the 5G high-frequency spectral range with the metasurface formed with coupled resistors. In addition, the 24.25-27.5GHz frequency range, one of the high-frequency 5G bands used by selected countries such as the European Union and China, was preferred. The minor aim of this study is that the usage of coupled elements as resistors may have the ability to increase the absorption bandwidth and magnitude. Comprehensive simulations were performed using the finite integration technique (FIT) utilized by the CST Microwave Studio program to investigate the absorber performance and other relevant parameters. The unit cell design is created metal-substrate-metal structures as asymmetric, single-layer, and easy to implement. The absorption responses are investigated according to the oblique incidence angle, polarization angle for TE & TM modes. The suggested MMA provided an absorbency response above 87.6% in the frequency range 24.20-27.30GHz under normal incidence. Moreover, to comprehend the physical mechanism on absorption, the top and bottom surfaces of the absorber's electric field and surface current distributions are assessed. The designed MMA resulting in relatively high performance and polarization insensitive is helpful for electromagnetic interference (EMI) shielding of 5G signals in the FR2/mmWave frequency regime.

¹ Seher Şeyma ARSLAN MADAK ([Orcid ID: 0009-0009-5795-8221](https://orcid.org/0009-0009-5795-8221)), Ramazan TOPKAYA ([Orcid ID: 0000-0002-5376-0199](https://orcid.org/0000-0002-5376-0199)), İğdir University, Faculty of Engineering, Department of Electrical and Electronics Engineering, İğdir, Türkiye

² Ahmet TEBER ([Orcid ID: 0000-0002-7361-2302](https://orcid.org/0000-0002-7361-2302)), Bayburt University, Vocational School of Technical Sciences, Department of Electricity and Energy, Bayburt, Türkiye

*Corresponding Author: Ahmet TEBER, e-mail: ahmetteber@bayburt.edu.tr

This study was produced from Seher Şeyma ARSLAN MADAK's Master's thesis.

INTRODUCTION

The 5G technologies' goals are not only to provide mobile broadband service but also to offer essential developments with a much more comprehensive range of applications, such as frequency-selective devices in complex wireless electronic systems and the Internet of Things (IoT) (Naqvi et al., 2022). In 5G technology, there exist additional 5G frequency bands in addition to the low and medium frequency band in the sub-7GHz range, which is defined as frequency range 1 (FR1), additional 5G frequency bands are being available. For this purpose, higher frequency bands over 24 GHz, also known as frequency range 2 (FR2)/mmWave, are actively become available by 5G technology for a variety of applications. The fundamental goal of introducing more spectrum is to overcome the practical challenges brought on by crowding, throughput, and capacity below 7 GHz. (Sleiman, 2021). In the historical process, 5G has dominated scenarios that push the boundaries of wireless communication, with ultra-high speeds, extremely low latency and incredibly high reliability.

In the first 5G spectrum meeting, the 24 GHz (including 24.25–24.45GHz and 24.75–25.25GHz) and 28 GHz (including 27.5–28.35GHz) bands, such a wide bandwidth in the mmWave have been approved for 5G by the Federal Communications Commission (FCC) (Anonymous, 2018). In addition, above FR1 24.25-27.5 GHz has been approved by the European parliamentary research service (EPRS) (Anonymous, 2023). It should be noted that the application and auction procedures for the next open meeting of licenses for the Upper Microwave Flexible Use Service (UMFUS) in the 28 GHz and 24 GHz bands have been created by the FCC. The focus of the researchers might then shift to creating creative solutions for these frequencies. For uniform network coverage in 5G technology, more transmission antennas are necessary compared to 4G. It requires the installation of denser 5G base stations at certain distances. Sensitive equipment in the industrial, scientific, and medical industries may malfunction because of the higher electromagnetic (EM) radiation dosages delivered by these 5G base stations. In some scenarios, 5G mobile phone signals need to be isolated or absorbed for security and confidentiality. Therefore, it also demands EM interference (EMI) protection of 5G signals in the FR2/mmWave frequency regions.

For engagement with wireless communication devices, metamaterial absorbers (MMAs) based on the resonance principle have been investigated such as emitters (Lee et al., 2019), filters (Chen et al., 2018), sensors (Kairm et al., 2014), photodetectors (Li et al., 2019), photovoltaic solar cells (Wang et al., 2012), and infrared camouflage (Lee et al., 2019). Although there are significant studies on MMA designs for microwave (Li et al., 2019; Bilal et al., 2020; Amiri et al., 2020), terahertz (Didari-Bader & Saghaei, 2023; Ma et al., 2023), visible (Chao et al., 2023; Guo et al., 2023) and ultraviolet (Wu et al., 2022; Alsharari et al., 2023) frequencies in the literature, there is still a relative gap in this regard for 5G high frequencies (especially between 24 GHz and 28 GHz bands) (Naqvi et al., 2022). Furthermore, investigations on narrowband, broadband, and ultra-wideband absorbers have limits due to their expensive and sophisticated materials for EM wave enhancement and complicated geometric forms. (Wen et al., 2013; Banadaki et al., 2017; So et al., 2021; Wang et al., 2021). More comprehensive comparisons are given in the discussion section. More recently, it has been shown that in broadband metamaterial absorber designs, far from geometry complexity, it is easier to obtain a high impedance surface absorber by adding lumped resistors (LRs), inductors or capacitors either series or parallel configurations (Chen et al., 2015; Shi et al., 2017). After the aforementioned justifications, the primary goal of this work is to overcome the gap of metamaterial absorbers in broadband for 5G high frequency additional region. This reveals the originality of this study.

In this paper, a novel absorber using lumped resistors operating at 24.20GHz-27.30GHz frequency band for 5G applications is proposed. The investigated lumped resistors' value are chosen to be modeled as the value of RF type resistors, which are easily provided by the market. The absorption is achieved above 87.6%. It means that the suggested MMA has high performance. The substrate material (FR4) with the thickness of $0.129\lambda_0$ ($h=1.6\text{mm}$) where λ_0 is the wavelength based on lower absorption frequency, is utilized to create the absorber is cost-effective, and the structure is simple to design. The general design parameters and procedure for the operation of the MMA in the investigated frequency spectrum are presented in the Materials and Methods section. Results such as the simulated and calculated parameters of the absorber and the physical absorption mechanism underlying the absorption are presented in the Results and Discussion section. Eventually, our results are compared with other articles of 5G in the literature.

MATERIALS AND METHODS

In this section, the materials, design parameters and stages of the presented metamaterial absorber are given in detail. First of all, materials and design procedure are given, then the methodology related to the absorption background is proposed.

Materials and Design Procedure

The symmetric MMA structure, which consists of five stages, contains a single layer of copper (pure)-FR4 substrate-copper (pure) configuration where FR4 is a composite material consisting of a flame resistant (self-extinguishing) glass-reinforced epoxy resin binder and a woven fiberglass fabric. The FR4 (lossy) is selected from the library of CST Microwave Studio program as a substrate material with the parameters of $\epsilon=4.3$, loss tangent(δ)=0.025, $\mu=1$, the electrical conductivity (σ)=0.025 [S/m], and thermal conductivity (κ)=0.3 [W/K/m]. FR4 thickness is chosen $h=1.6\text{mm}$ ($=0.129\lambda_0$ where λ_0 is the wavelength based on the lower frequency of microwave absorption). In the unit cell of MMA, copper is also preferred to use on top and bottom of the MMA including 35microns thickness and a conductivity of $\sigma=5.96\times 10^{-7}\text{S/m}$ as a metallic layer. The bottom surface is entirely covered by the pure copper.

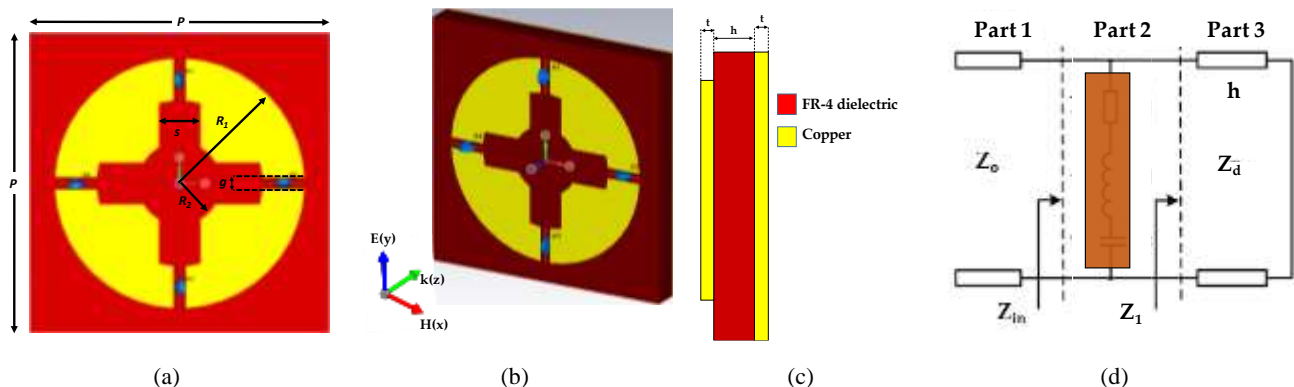


Figure 1. Metamaterial absorber with design parameters (a) frontal view, (b) perspective view, (c) lateral view, and (d) equivalent circuit representation

As is well known, comprehensive optimization of geometric parameters, such as substrate thickness, size, and shape, is necessary to get the optimal configuration with acceptable absorption capabilities. CST Microwave Studio 3D interactive modeling tool is used to create metasurface, substrate and metallic plate, which entirely covers the substrate. In our design, a square structure with a thickness of 35 microns was created in the xoy plane on the xyz coordinate system, with the dimensions in Table 1. This square structure's primary material was copper from the CST library. Similarly, the structure to be used as a substrate was created along the +z axis with the help of the modeling tool, and FR4 was

selected as the material type from the library. Then, the metasurface structure (35 microns thick) embedded on the FR4 surface was created by following the steps in Figure 2. It should be noted that the material parameters of copper and FR4 used in the design are given above.

Modeling of the metasurface was carried out in five steps. First, Stage 1 was created with a circular plate (35-micron thickness) of radius R_1 . Afterward, a concentric circular plate with a radius of 4 mm was extracted from the main plate. Stage 2 was created by removing perpendicular rectangular blocks (0.6 mm in width and 12 mm in length) from the resulting structure. In the third stage, a circular plate with a 2mm radius was removed from the circular plate with an outer radius of 4.2mm, similar to the second stage. Afterward, perpendicular rectangular structures (2 mm wide and 9 mm long) were removed from the created bagel structure, and Stage 3 was completed. The fourth stage was completed by combining the structures in the second and third phases. In the last stage (fifth stage), the MMA structure is created by adding bulk resistors (Figure 1). Equivalent circuit representation has also been added for absorption descriptions. Table 1 contains a list of design parameters.

Two concentric but different sizes of circular structures were created. Then, rectangular blocks in horizontal and vertical positions were subtracted from these two different circular structures. After these processes, these two concentric circular structures were combined. Finally, by adding lumped resistors, the MMA structure is created (Figure 1). The serially connected lumped resistances were defined as the width ($g = 0.6$ mm), length (2 mm), and lumped resistors' thickness (equal to the thickness of the metasurface structure as 35 microns). An edge lumped resistor is defined by a start point and an endpoint in the design. The resistor modeling was carried out in CST Microwave Studio using the RF resistor model approach with the parameters of the parasitic capacitor ($C_p=0.04$ pF), the inductance associated with the resistor value of $L_s (=0.78$ nH), the resistor series lead inductance ($L_{lead}=0.09$ nH) and shunt capacitance ($C_{shunt}=0.015$ pF). Other properties are listed as follows: Resistance in Ohms is 50, simulation temperature in Celsius is 26.85, first and second-order temperature coefficients are zero, and temperature at which parameters are extracted ($T_{nominal}$) is 26.85 in Celsius. The equivalent circuit representation is also attached for the absorption explanations. Table 1 contains a list of the design parameters.

Table 1. Best-performing MMA design parameters for absorption

g (mm)	h (mm)	P (mm)	R_1 (mm)	R_2 (mm)	s (mm)	R(ohm)	t (mm)
0.6	1.6	14.4	6	2	2	51	0.035

Meanwhile, the best absorption results were obtained by performing absorption simulations at different stages (from Stage 1 to Stage 5) illustrated in Figure 2. Based on each stage, the absorption results obtained is going to be discussed in the Results and Discussion section.

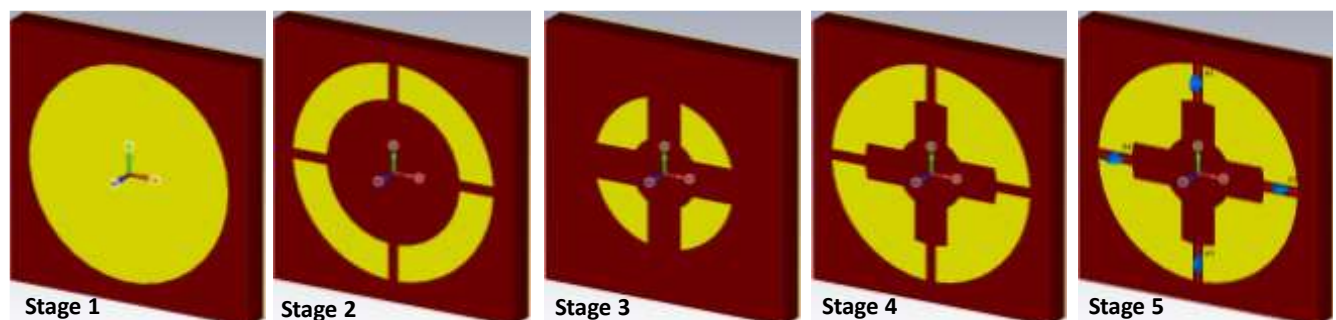


Figure 2. The design stages of the suggested metamaterial absorber

Absorption Mechanism

In order to best (or better) absorbency results, the surface impedance of the metal array should be able to match with the free space wave impedance. The absorption of the metamaterial with an impedance matching between air and MMA can be defined as follows:

$$A(\omega) = 1 - R(\omega) - T(\omega) = 1 - |S_{11}(\omega)|^2 - |S_{21}(\omega)|^2 \quad (1)$$

where $A(\omega)$, $R(\omega)$, and $T(\omega)$ represent the absorbance, reflectance, and transmittance, respectively (Bhattacharyya and Vaibhav, 2014). $R(\omega)$ and $T(\omega)$ are determined from the frequency dependent scattering parameters of $S_{11}(\omega)$ and $S_{21}(\omega)$, respectively. The maximum absorption rate can be maximized by the reflection and transmission coefficients, simultaneously. Because of the thickness of the copper surface, the bottom layer is thick enough to block the transmission of the incident wave, so that $T(\omega)$ will be zero. Then, the absorbency could be obtained as flows:

$$A(\omega) = 1 - R(\omega) = \left| \frac{Z_{in}(\omega) - Z_0}{Z_{in}(\omega) + Z_0} \right| \quad (2)$$

where $Z_{in}(\omega)$ is the characteristic input impedance, while Z_0 is the free space characteristic impedance. In order to optimize the MMA dimensions, the equivalent circuit model has been introduced based on transmission line theory (Nguyen and Lim, 2018), as shown in Figure 1d. The first region of the transmission line has a characteristic impedance of Z_0 . The second region includes RLC combinations in a parallel configuration with the impedance of Z_m , representing the components on the metal top layer. The third region is the shorted transmission line, modeling the FR4 substrate with a length of h (mm) and the Z_d impedance. The input impedance can be calculated for the parallel configuration impedance of the MA and the shorted transmission line as follows:

$$\frac{1}{Z_{in}(\omega)} = \frac{1}{Z_m(\omega)} + \frac{1}{Z_d(\omega)} \quad (3)$$

$$\frac{1}{Z_m(\omega)} = \frac{1}{R_1 + j\omega L_1 + \frac{1}{j\omega C_1}} + \frac{1}{R_2 + j\omega L_2 + \frac{1}{j\omega C_2}} + \frac{1}{R_3 + j\omega L_3 + \frac{1}{j\omega C_3}} + \frac{1}{R_4 + j\omega L_4 + \frac{1}{j\omega C_4}} \quad (4)$$

$$\frac{1}{Z_d(\omega)} = j \sqrt{\frac{\omega_r \omega_0}{\epsilon_r \epsilon_0}} \tan(kh) \quad (5)$$

$$k = \frac{k_0}{\sqrt{\epsilon_r \omega_r}} \quad (6)$$

Here, ϵ_r is the relative permittivity, while μ_r is the permeability, and k is the wave number travelling through the dielectric substrate, respectively. ϵ_0 is the relative permittivity of free space, while μ_0 and k_0 are free space's permeability and wave number, respectively. The question is: How can researchers ensure impedance matching in investigated frequency regions? The real and imaginary parts of the normalized input impedance (Z) would be 1 and 0, respectively, as an answer. So, Z can be defined as follows (Jang et al., 2014):

$$Z = \sqrt{\frac{(1+S_{11}^2) - S_{21}^2}{(1+S_{11}^2) + S_{21}^2}} \quad (7)$$

The physical absorption mechanism needs to be clarified by obtaining EM constitutive parameters (permittivity and permeability) using S_{11} parameters as follows (Sy Tuan and Thi Quynh Hoa, 2019).

$$\epsilon_{eff} = 1 + \frac{2j}{k_0 h} \frac{S_{11}-1}{S_{11}+1} \quad (8)$$

$$\mu_{eff} = 1 + \frac{2j}{k_0 h} \frac{S_{11}+1}{S_{11}-1} \quad (9)$$

where the wave-number is k_0 where the distance travelled by the incident wave is h . These constitutive parameters figure out an answer to whether the absorbcency occurs because of either an electric or a magnetic resonance (or both).

The frequency domain solver (tetrahedral mesh) of the finite integration technique (FIT) is used to simulate and optimize the absorption performances of the suggested design in the CST software. Periodic boundary conditions are utilized along the x - and y - directions, whereas the open (add space) boundaries are set along the direction of propagation waves, the z -direction (Figure 3). Due to the impedance matching between the resonator and free space, electromagnetic waves pass through the generated metasurface on top when they strike the MMA surface. The dielectric substrate layer in the middle captures EM waves and traps them inside the structure. The metallic layer behind it completely covers the substrate layer and acts as a perfect reflector for the EM waves, preventing signal transmission to the other side.

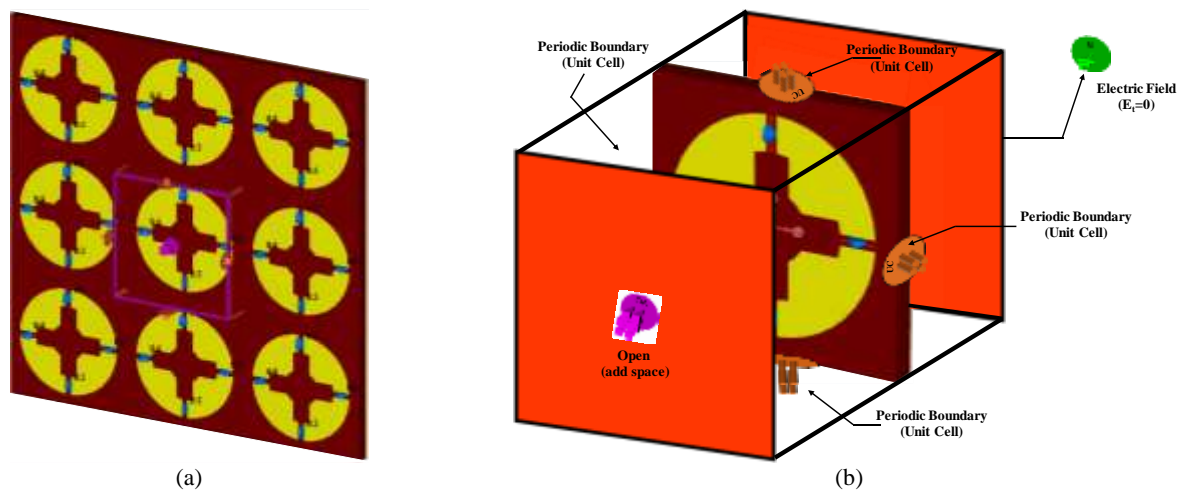


Figure 3. (a) Periodic boundary conditions along x - and y - directions (b) simulation setup with boundary conditions

RESULTS AND DISCUSSION

Parameters and analysis results obtained as a result of the simulation are examined in categories in this section.

Absorption Based on Design Stages

According to the design stages, the impact of architectural changes on electromagnetic wave absorption for 5G is examined. The proposed design (in Figure 1) is briefly created by following the necessary steps outlined in the geometry given in Figure 4. Figure 4a-e represent the absorbcency for each stage in detail, while Figure 4f exhibits the combined absorption results to compare one to another.

Stage 1 consists of a circular structure with a radius of 6 mm centered at the origin. As shown in Figure 4a, over 80% absorption was observed in a very narrow band (below 25GHz) in the scanned frequency range. However, this absorption does not reach an acceptable value. The structure in the second stage was obtained with the 0.6mm wide structure extracted from the circular ring with an outer radius of 6mm and an inner radius of 4mm, in accordance with the design geometry. However, it is clear that the absorption remains below 80%.

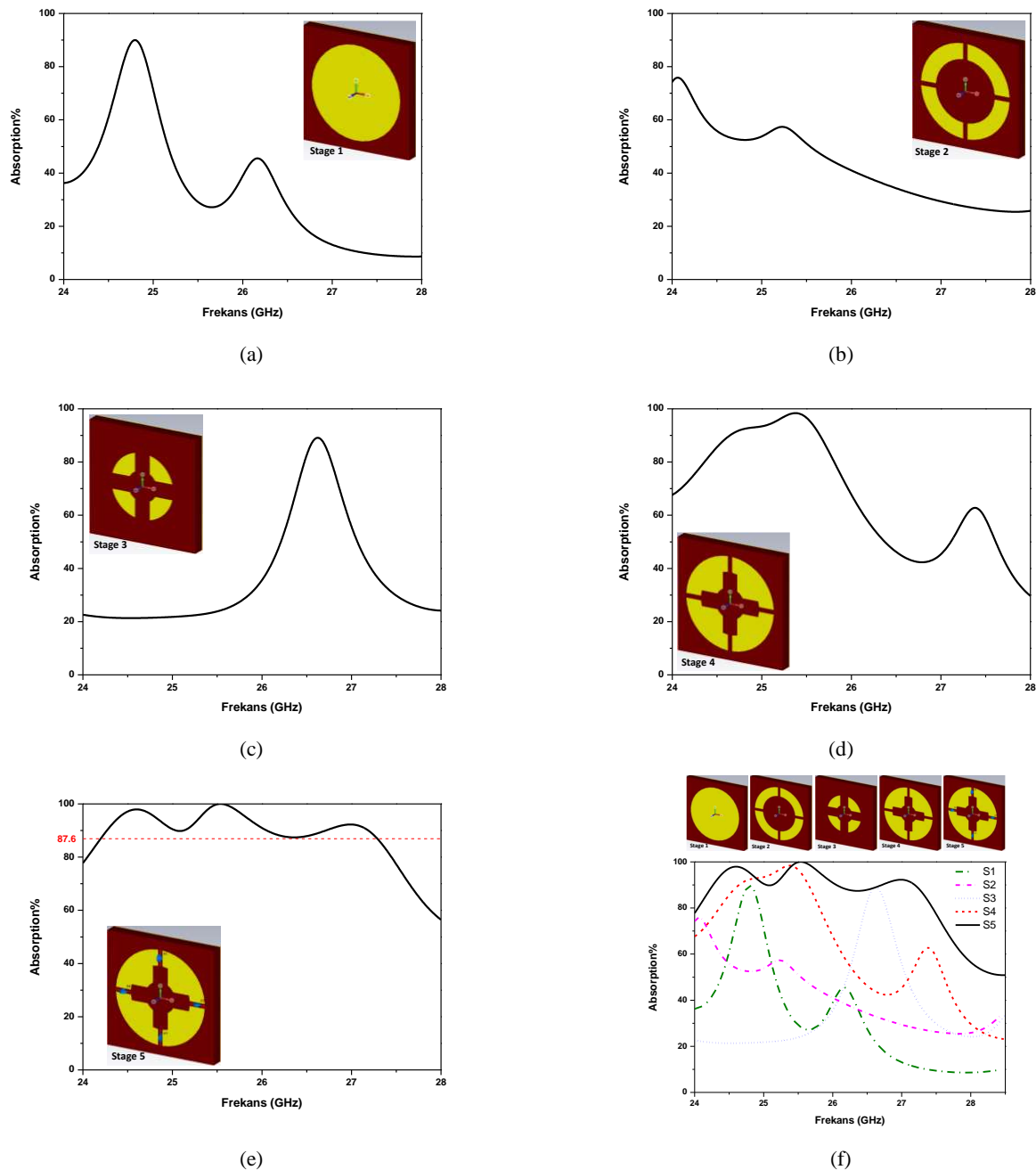


Figure 4. (a-e) Absorption results obtained according to the design stages (f) Combined absorption results

Again, in accordance with the design geometry, the absorption of the third stage structure was observed above 80% in the 26.5-27GHz frequency range, with the 2mm wide structure removed from the circular ring with an outer radius of 4.2mm and an inner radius of 2mm. However, this absorption value is definitely not sufficient and efficient for the band in our area of interest, as it was in the previous stages. The geometry in the fourth stage was combined with the structures of the second and third stages. Even though the absorption results were improved over the absorption bands from Stages 1 to 3, the absorption results still showed that acceptable absorption could not be achieved. Over 87.6% absorption achieved in the fifth stage is achieved between 24.20GHz and 27.30GHz for this study, mainly investigating focused frequency band. Since the aforementioned processes are completed, the absorption for 5G band is accomplished by getting to fifth stage of the suggested metamaterial absorber design.

Oblique Incidence Angle-Based Absorption for TE and TM Mode

The absorption spectral changes is plotted under normal incidence for both TE and TM polarizations in Figure 5. The suggested MMA reveals three distinct absorption points at 24.60GHz, 25.53GHz, and 27.00GHz, corresponding to the reachable absorptivities of 97.90%, 100%, and 92.43%, respectively. More importantly, the high absorbency larger than 87.6% under normal incidence for TE and TM mode is achieved in a wide frequency range of 24.20GHz to 27.30GHz, covering high frequency 5G band except the interval of 27.30GHz-27.5GHz.

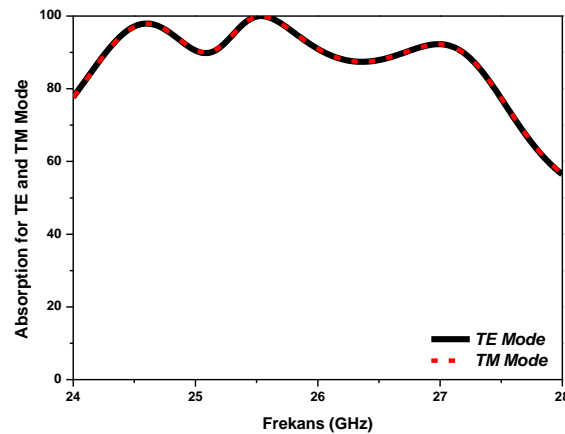


Figure 5. Absorption under normal incidence for TE and TM Mode

In addition, oblique incidence angles based absorption spectral changes are illustrated for TE and TM mode, separately, in Figure 6a and Figure 6b. It is obvious that the designed MMA is incidence angle dependent. Namely, it is sensitive depending on the incidence angle for both mode. Above 80% absorption, resonance points and absorption bandwidth vary. It has been observed that it has a narrower absorption band, while the absorption up to 40° is above 80%. Above 40° , the absorption band shows a serious decrease. The TM mode's absorption curves differ greatly from the TE mode's from Figure 6b.

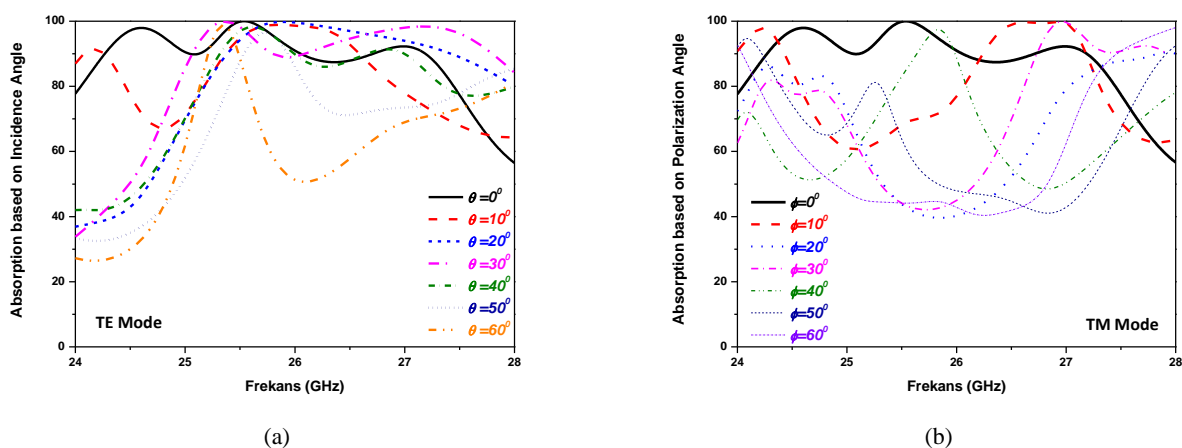


Figure 6. Oblique incidence angle based absorption (a) for TE Mode and (b) for TM Mode

Polarization Angle-Based Absorption for TE and TM Mode

Figure 7 indicates the simulated polarization angle-based absorption results for TE and TM mode. The absorbency remains unchanged depending on different polarization angles, demonstrating that a polarization insensitive MMA is achieved under oblique incidence angle for both mode.

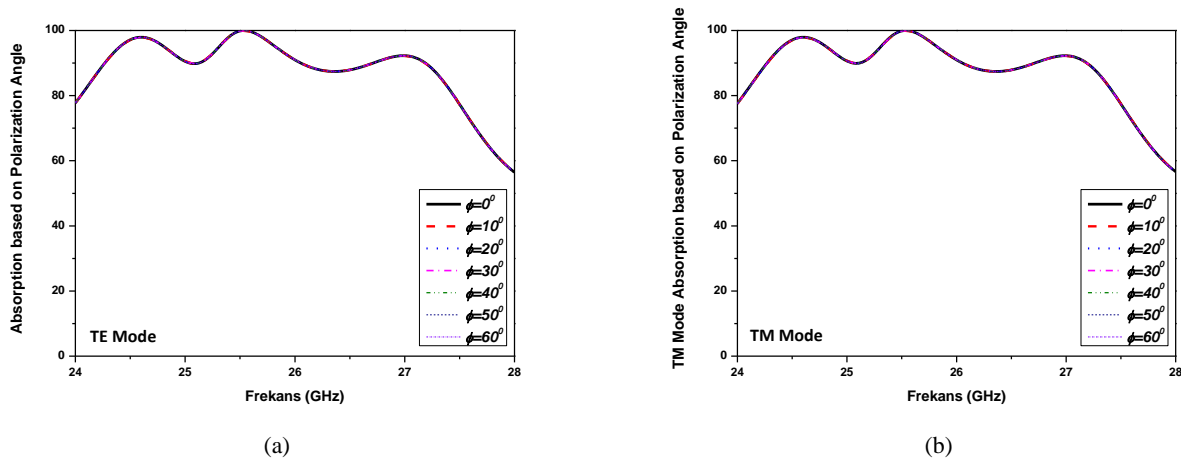


Figure 7. Absorption based on polarization angle (a) for TE Mode and (b) for TM Mode

Effective Permittivity and Permeability

Effective electromagnetic constitutive parameters of ϵ_r and μ_r as complex parameters are retrieved to provide the physical absorption mechanism in detail under normal incidence for TE mode. From Equation 8 and 9, these parameters are obtained, including the real and the imaginary parts. The extracted effective real and imaginary parts of permittivity and permeability are plotted in Figure 8a and Figure 8b. The negative values of for both the imaginary parts of permittivity and permeability obtained confirms that the absorption of suggested MMA mainly occurs by the electric and magnetic resonance. This result is also confirmed with the division of MMA into regional cells by using electric field and surface current distributions in Figure 9.

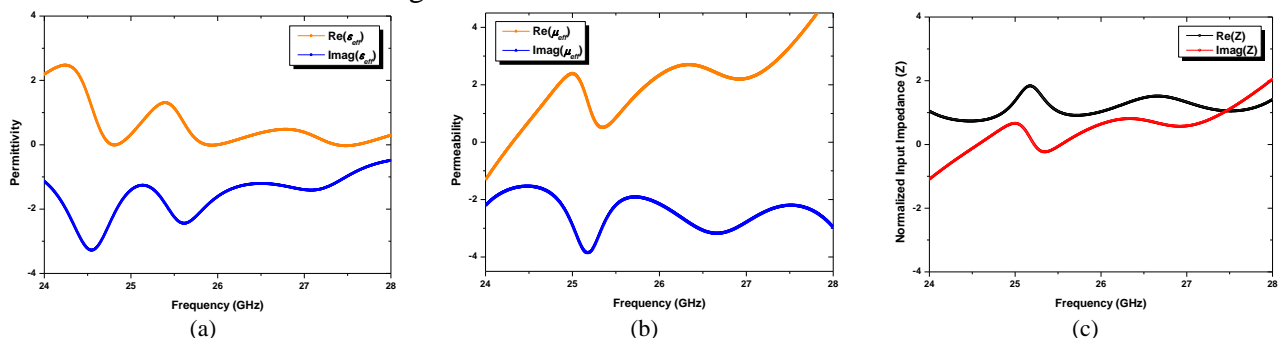


Figure 8. The extracted (a) effective permittivity, (b) effective permeability, and (c) normalized input impedance

The calculated normalized input impedance (Z), including real and imaginary parts is shown in Figure 8c. It is observed that the real part of Z oscillates around 1, while imaginary part of Z oscillates around 0 in the frequency range under focus. These results confirm that the impedance matching is successfully achieved. Moreover, it shows that the absorption mechanism of the designed MMA can be explained by the attached lumped resistors, the effective medium interference theory.

Electric Field and Surface Current Distributions

It is important to understand the physical absorption mechanism in MMA designs and to validate it together with the electromagnetic constitutive parameters. For that purpose, the electric field on the top surface of the MMA and the surface current distributions on top and bottom surfaces of MMA were examined at the frequencies at which resonance occurred. At this point, from the electromagnetic constitutive parameters mentioned above, it is worth remembering again that both electric and magnetic resonance are effective in the physical absorption mechanism, since the imaginary parts of the effective permittivity and permeability parameters are negative. It is now necessary to verify this result obtained

from the electromagnetic constitutive parameters by examining the electric field and surface current distributions on the metamaterial surface in this section.

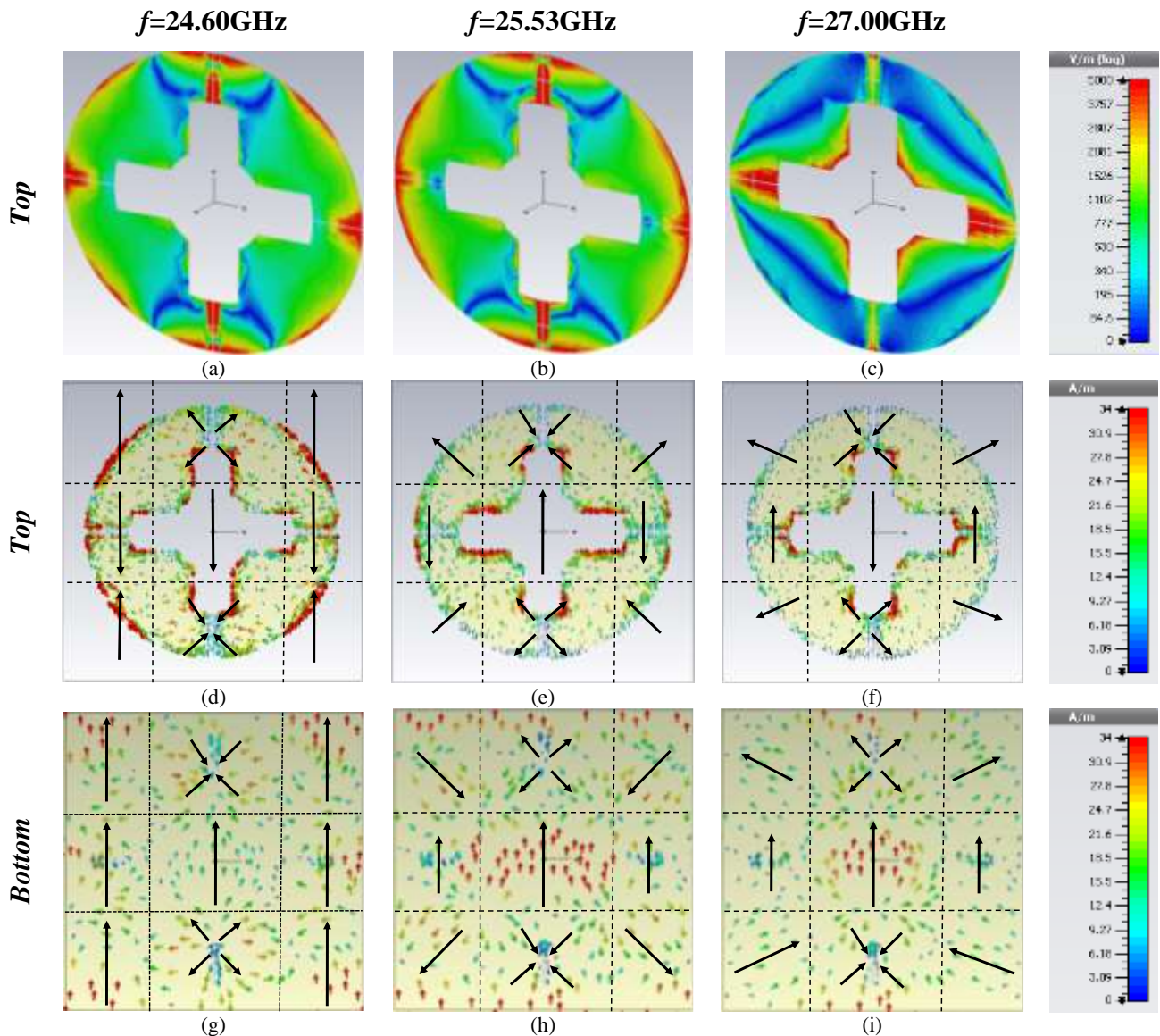


Figure 9. At three peak resonance points of the absorption spectra: (a-c) Electric field distributions on the top surface of the suggested MMA, (b) Surface current distributions on the top surface of the suggested MMA, and (c) Surface current distributions on the bottom surface of the suggested MMA

The electric field and surface current distributions on XoY plane are simulated at the three resonance frequencies of 24.60GHz, 25.53GHz, and 27.00GHz under normal incidence. According to the electric field in Figure 9a-c, the resonant absorption at 24.60GHz and 25.53GHz is mainly generated at the edges of the surface and the lumped resistors. Moreover, the resonant absorption at 27.00GHz is mainly generated at the inner edges of the surface, while in the horizontal axis lumped resistances, more electric field was generated than in the vertical axis lumped resistances. It was also concluded that lumped resistors contributed to the absorption.

The surface current distributions of top surface of the suggested MMA is presented in Figure 9d-f, while Figure 9g-i represents the surface current distributions for bottom surface of the suggested MMA. The surface current distributions were analyzed by dividing the unit cell into regions in a 3x3 matrix format (Table 2). The situations of the surface current distributions on the upper and lower surfaces over this matrix was examined as follows. Considering that parallel surface currents originate from electrical resonance (ER) and anti-parallel surface currents originate from magnetic resonance

(MR), it will be explained regionally which type of resonance has an effect on absorption by using ER and MR notations.

Table 2. The regional distributions of electric and magnetic resonances

$f=24.60\text{GHz}$	$f=25.53\text{GHz}$	$f=27.00\text{GHz}$
$\begin{bmatrix} ER & MR & ER \\ MR & MR & MR \\ ER & MR & ER \end{bmatrix}$	$\begin{bmatrix} MR & MR & MR \\ MR & ER & MR \\ MR & MR & MR \end{bmatrix}$	$\begin{bmatrix} ER & MR & ER \\ ER & MR & ER \\ MR & MR & MR \end{bmatrix}$

The structure that creates a multi-surface current loops between the upper and lower metallic layers confirms that the absorption takes place with the effect of multi-order electric and magnetic resonance. In this way, it is also concluded that it is in strong agreement with the result obtained from the electromagnetic constituent parameters.

Parametrical Investigation

The absorption changes based on the few dimension parameters in Figure 10a through Figure 10d are simulated at the unit cell size (P), the substrate thickness (h), the resistor values (R), and the radius of the outer ring (R_1). For the highest absorption and the widest frequency range depending on these parameters, the optimized parameters are chosen as following: P=14.4mm, h=1.6mm, R=51 Ω , and R₁=6mm.

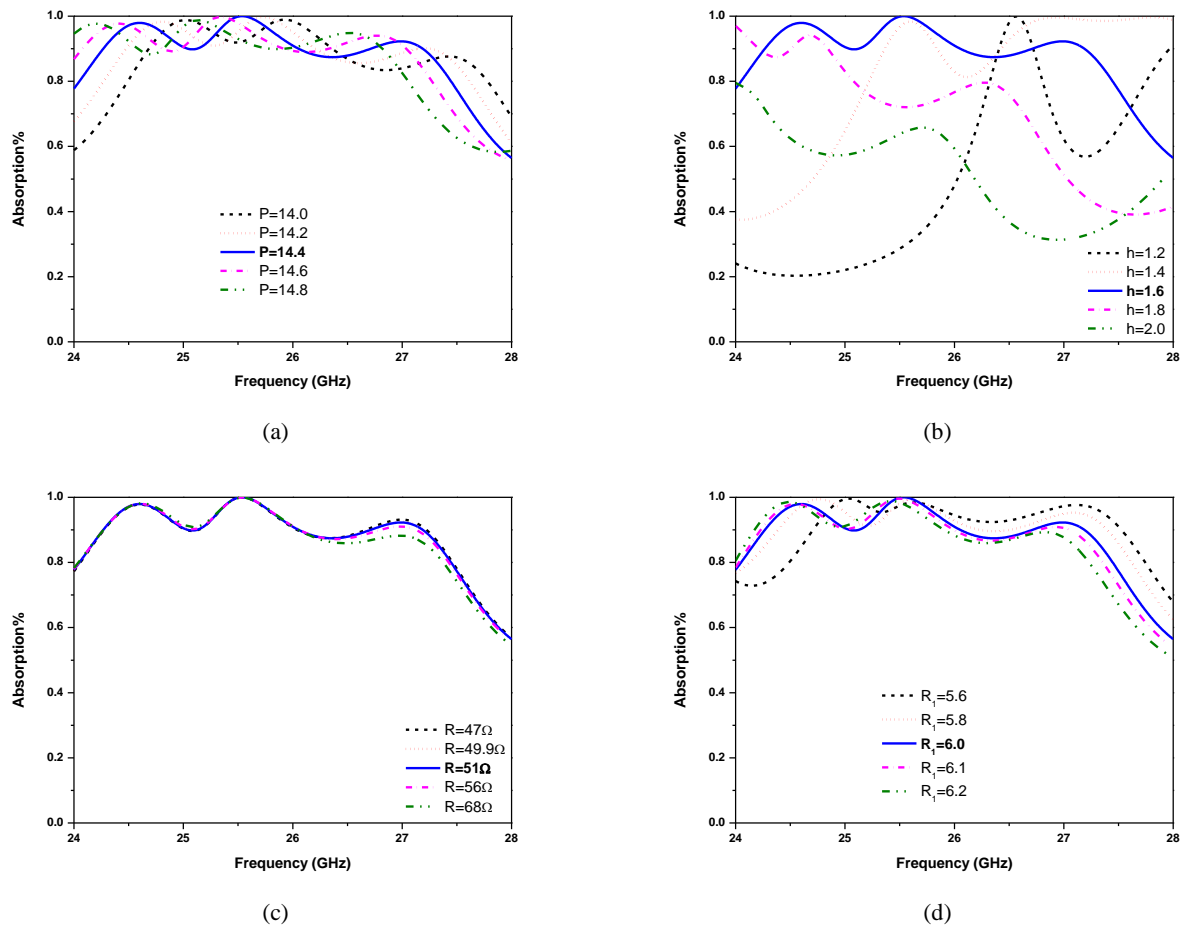


Figure 10. Absorption changes of the designed metamaterial absorber for various parameters: (a) P=14.0mm-14.8mm, (b) h=1.2mm-2.0mm, and (c) R=47 Ω , 49.9 Ω , 51 Ω , 56 Ω , and 68 Ω the resistor values, and (d) R_1 =5.6mm-6.2mm

Analysis of Performance of the Designed MMA

The performance of suggested MMA is compared with similar studies regarding 5G high-frequency bands (Table 3). To the best of knowledge in the literature, it is seen that there are few publications in the band ranges accepted by the FCC and the European parliamentary research service. The proposed MA structure stands out as an absorber in the band range accepted by the FCC and European parliamentary research service compared to presented publications. In addition, high wideband absorbency, thinner- simplistic designation, polarization-insensitive are listed as advantages. These important features are due to the combinations of electrical thickness, dielectric substrate, copper ground plane, resonance by lumped resistors, and EM interaction between incident wave and absorber. In addition, experimental analysis can be performed after the prospective generation of the proposed MMA.

Table 3. Performance comparison of the designed MMA with 5G related studies

References	Thickness (mm)	Freq. Band (GHz)	Polarization Sensitiveness	LR	Absorption BWs	Incident Angle Dependency	Absorption
(Li et al., 2019)	0.25 ($0.56\lambda_0$)	27.5-28.35	insensitive	No	3.56GHz 1.73 GHz (Double Resonance)	45°	-42.34 dB -33.43 dB
(Amiri et al., 2020)	1.0 (N/A)	15-60	sensitive	No	31.4 GHz	20°	Above 90%
(Akarsu et al., 2022)	0.787 (N/A)	27.67-43.87	N/A	No	16.2 GHz	20°	Above 95%
(Ruan et al., 2023)	2.2 (N/A)	11.42-42.8	insensitive	No	31.6 GHz	45°	-29.7 dB -32.0 dB
(Xiaoyong et al., 2020)	1.35 (N/A)	23-47	insensitive	Resistor	24 GHz	N/A 40°	-47 dB
Proposed Study	1.6mm ($0.129\lambda_0$)	24.20-27.30	insensitive	Resistor	3.10 GHz	with narrow bandwidths for TE Mode	Above 87.6%

CONCLUSION

In this study, we designed and numerically analyzed a polarization-insensitive MMA using lumped resistors with relatively high efficiency operating in one of the high frequency 5G ranges defined by the FCC and EPRS. The designed MMA achieved an absorption of over 87.6% in the 24.20-27.30 GHz frequency range, with maximum absorption of 97.90%, 100% and 92.43% at the three resonant frequencies of 24.60GHz, 25.53GHz, and 27.00GHz, respectively. It was observed that the designed MMA was not independent of oblique incidence angle except normal incidence. In addition, the resonance frequencies shifted towards higher and/or lower frequencies for TE and TM modes based on oblique incidence angle. It was confirmed that the physical absorption mechanism is due to electric and magnetic resonances, comparing EM constitutive parameters and the electric field & surface current distributions. This simulated MMA can be a good candidate for electromagnetic interference (EMI) shielding of 5G signals.

Conflict of Interest

The article authors declare that there is no conflict of interest between them.

Author's Contributions

Seher Şeyma Arslan Madak ve Ahmet Teber are proposed the idea, performed the simulation, analysis/computation absorption. The manuscript is written by Seher Şeyma Arslan Madak with the help

of Ahmet Teber. In addition, Ahmet Teber and Ramazan Topkaya contributed to this study with fruitful discussions and reviewed the manuscript.

REFERENCES

- Anonymous. (2018). Federal Communications Commission (FCC), FCC Establishes Procedures for First 5G Spectrum Auctions. URL: <https://www.fcc.gov/document/fcc-establishes-procedures-first-5g-spectrum-auctions-0> (Accessed date: May 20, 2023).
- Anonymous. (2023). European Parliamentary Research Service (EPRS), 5G Frequencies. URL: <https://map.sciencemediahub.eu/5g#m=4/912.84457/845.58674,p=14> (Accessed date: May 20, 2023).
- Akarsu, G., Nakmouche, M.F., Fawzy, D.E. & Allam, A.M.M.A. (2022). A Novel Ultra-Wideband Metamaterial-Based Perfect Absorber for 5G Millimeter-Wave Applications. In: 9th International Conference on Electrical and Electronics Engineering (ICEEE), IEEE (129-132). Alanya, Turkey. <https://ieeexplore.ieee.org/abstract/document/9772547>
- Alsharari, M., Han, B.B., Patel, S.K., Surve, J., Aliqab, K. & Armghan, A. (2023). A Highly Efficient Infinity-Shaped Large Angular-and Polarization-Independent Metamaterial Absorber. *Symmetry*, 15(2), p.352.
- Amiri, M., Tofigh, F., Shariati, N., Lipman, J. & Abolhasan, M. (2020). Ultra wideband dual polarization metamaterial absorber for 5G frequency spectrum. In: 14th European Conference on Antennas and Propagation (EuCAP), IEEE (1-5). Copenhagen, Denmark. <https://ieeexplore.ieee.org/xpl/conhome/9127589/proceeding>
- Banadaki, M.D., Heidari, A.A. & Nakhkash, M. (2017). A metamaterial absorber with a new compact unit cell. *IEEE Antennas and Wireless Propagation Letters*, 17(2), 205-208.
- Bhattacharyya, S. and Vaibhav Srivastava, K. (2014). Triple band polarization-independent ultra-thin metamaterial absorber using electric field-driven LC resonator. *Journal of Applied Physics*, 115(6), 064508.
- Bilal, R.M.H., Baqir, M.A., Choudhury, P.K., Ali, M.M., Rahim, A.A. & Kamal, W. (2020). Polarization-insensitive multi-band metamaterial absorber operating in the 5G spectrum. *Optik*, 216, 164958.
- Chao, C.T.C., Kooh, M.R.R., Lim, C.M., Thotagamuge, R., Mahadi, A.H. & Chau, Y.F.C. (2023). Visible-range multiple-channel metal-shell rod-shaped narrowband plasmonic metamaterial absorber for refractive index and temperature sensing. *Micromachines*, 14(2), 340.
- Chen, J., Huang, X., Zerihun, G., Hu, Z., Wang, S., Wang, G., Hu, X. & Liu, M. (2015). Polarization-independent, thin, broadband metamaterial absorber using double-circle rings loaded with lumped resistances. *Journal of Electronic Materials*, 44, 4269-4274.
- Chen, X., Chen, X., Wu, Z., Zhang, Z., Wang, Z., Heng, L., Wang, S., Zou, Y. & Tang, Z. (2018). An ultra-broadband and lightweight fishnet-like absorber in microwave region. *Journal of Physics D: Applied Physics*, 51(28), 285002.
- Didari-Bader, A. & Saghaei, H. (2023). Penrose tiling-inspired graphene-covered multiband terahertz metamaterial absorbers. *Optics Express*, 31(8), 12653-12668.
- Guo, T., Li, F. & Roussey, M. (2023). Dielectric Cavity-Insulator-Metal (DCIM) Metamaterial Absorber in Visible Range. *Nanomaterials*, 13(8), 1401.
- Jang, T., Youn, H., Shin, Y.J. & Guo, L.J. (2014). Transparent and flexible polarization-independent microwave broadband absorber. *Acs Photonics*, 1(3), 279-284.

- Kairm, H., Delfin, D., Shuvo, M.A.I., Chavez, L.A., Garcia, C.R., Barton, J.H., Gaytan, S.M., Cadena, M.A., Rumpf, R.C., Wicker, R.B. & Lin, Y. (2014). Concept and model of a metamaterial-based passive wireless temperature sensor for harsh environment applications. *IEEE Sensors Journal*, 15(3), 1445-1452.
- Lee, N., Kim, T., Lim, J.S., Chang, I. & Cho, H.H. (2019). Metamaterial-selective emitter for maximizing infrared camouflage performance with energy dissipation. *ACS applied materials & interfaces*, 11(23), 21250-21257.
- Li, Y., Ren, P. & Xiang, Z. (2019). A dual-passband frequency selective surface for 5G communication. *IEEE Antennas and Wireless Propagation Letters*, 18(12), 2597-2601.
- Li, J., Zhao, C., Liu, B., You, C., Chu, F., Tian, N., Chen, Y., Li, S., An, B., Cui, A. & Zhang, X. (2019). Metamaterial grating-integrated graphene photodetector with broadband high responsivity. *Applied Surface Science*, 473, 633-640.
- Ma, S., Zhang, P., Mi, X. & Zhao, H. (2023). Highly sensitive terahertz sensor based on graphene metamaterial absorber. *Optics Communications*, 528, 129021.
- Naqvi, S.A., Baqir, M.A., Gourley, G., Iftikhar, A., Saeed Khan, M. and Anagnostou, D.E. (2022). A Novel Meander Line Metamaterial Absorber Operating at 24 GHz and 28 GHz for the 5G Applications. *Sensors*, 22(10), 3764.
- Nguyen, T.T. and Lim, S. (2018). Angle-and polarization-insensitive broadband metamaterial absorber using resistive fan-shaped resonators. *Applied Physics Letters*, 112(2), 021605.
- Ruan, J.F., Meng, Z.F., Zou, R.Z., Pan, S.M. & Ji, S.W. (2023). Ultra-wideband metamaterial absorber based on frequency selective resistive film for 5G spectrum. *Microwave and Optical Technology Letters*, 65(1), 20-27.
- Shi, Y., Li, Y.C., Hao, T., Li, L. & Liang, C.H. (2017). A design of ultra-broadband metamaterial absorber. *Waves in random and complex media*, 27(2), 381-391.
- Sleiman D. (2021). RF and 5G new radio: top 5 questions answered. Access address: <https://www.exfo.com/es/recursos/blog/rf-5g-new-radio-top-5-questions/> (Access date: 05.20.2023).
- So, S., Yang, Y., Lee, T. & Rho, J. (2021). On-demand design of spectrally sensitive multiband absorbers using an artificial neural network. *Photonics Research*, 9(4), B153-B158.
- Sy Tuan, T. and Thi Quynh Hoa, N. (2019). Defect induced co-polarization broadband metamaterial absorber. *AIP Advances*, 9(5), 055321.
- Wang, Y., Sun, T., Paudel, T., Zhang, Y., Ren, Z. & Kempa, K. (2012). Metamaterial-plasmonic absorber structure for high efficiency amorphous silicon solar cells. *Nano letters*, 12(1), 440-445.
- Wang, X., Sang, T., Li, G., Mi, Q., Pei, Y. & Wang, Y. (2021). Ultrabroadband and ultrathin absorber based on an encapsulated T-shaped metasurface. *Optics Express*, 29(20), 31311-31323.
- Wen, D.E., Yang, H., Ye, Q., Li, M., Guo, L. & Zhang, J. (2013). Broadband metamaterial absorber based on a multi-layer structure. *Physica Scripta*, 88(1), 015402.
- Wu, L., Li, Z., Wang, W., Zhao, L. & Ruan, H. (2022). Ultra-Broadband Wide-Angle Polarization-Independent Enhanced Absorber with Ultraviolet to Far-Infrared Absorption Performance. *physica status solidi (b)*, 259(10), 2200158.
- Xiaoyong, L.E.I., Shuyun, H.U.O., Mengjun, W.A.N.G., Yan, L.I. & Erping, L.I. (2020). A compact ultra-wideband polarization-insensitive metamaterial absorber at 5G millimeter wave band. In: IEEE MTT-S International Conference on Numerical Electromagnetic and Multiphysics Modeling and Optimization (NEMO), IEEE (1-4). Hangzhou, China. <https://ieeexplore.ieee.org/abstract/document/9343462>